Tribological performance evidence on ternary and quaternary nitride coatings applied for industrial steel

J. C. Caicedo[a,b], W. Aperador[c], and Y. Aguilar[a]
[a]*Materials school, Universidad del Valle Ciudad Universitaria, Meléndez, A. A. 25360 Cali, Colombia, Powder Metallurgy and Processing of Solid Recycling Research Group, Universidad del Valle, Cali Colombia,*
[b]*Thin films group, Universidad del ValleCalle, 13 #100-00 Edificio 320, espacio 1026, Cali, Colombia,*
[c] *Departament of Engineering, Universidad Militar Nueva Granada, Carrera 11 No. 101-80, Fax:+57(1) 6343200, Bogotá, Colombia,*
e-mail: jcaicedoangulo1@gmail.com

Received 24 August 2012; accepted 17 April 2013

A diagnostic of mechanical and tribological behavior in ternary Ti-C-N and quaternary Ti-Nb-C-N films deposited onto Si (100) and 4140 steel substrates by r.f. magnetron sputtering processvarying negative bias voltage from 0 to -100 V,was done in this work. Growth parameters as power density, Ar/N_2 flow rate, and substrate temperature were keptconstant at the moment of the deposition. Introduction of Nb in the ternary Ti-C-N film was evaluated by X-ray diffraction (XRD) analysis.Quantitative elemental concentration depth profile by glow discharge optical emission spectroscopy (GDOES) and the morphology via scanning electron microscopy (SEM) were observed for the layers before the tests. Mechanical and tribological properties for both coatings were obtained by mean of nanoindentation measurements throughload versus displacement method, and scratch test using the critical load criterion, respectively. The failure modes from scratch test were observed via optical microscopy. XRD results show as the amount of Nb is increased into the quaternary phase, the preferred orientation change in the film due to the modification in the strain and lattice parameter (Caicedo et al., 2007). EDX results from previous work show the TiCN and TiNbCN layers were stoichiometric (Caicedo *et al*., 2007). Nanoindentation results reaching the elastic-plastic behavior of the TiCN and TiCN films with inclusion of Nb (TiNbCN), indicate not only the hardness and elastic modulus but also the critical load for the adhesive failure increase when increasing r.f negative bias voltage. An improvement of hardness and critical load around 60% and 28% for TiCN as well as 26% and 31%for TiNbCN, respectively, was associated to an increasing in the r.f negative bias voltage from 0 to -100 V.

Keywords: Hard coatings; bias voltage; elastic modulus; mechanical and tribological properties.

PACS: 62.20.de; 61.05.cf; 68.30.j; 68.35.Ja; 62.20.Qp.

1. Introduction

The development of superhard coatings, defined by hardness values above 40 GPa, has increased significantly during the last 15 years because of the interest in scientific and industrial applications. These superhard coatings possess an unusual combination of mechanical and chemical properties, such as high fracture toughness, high oxidation resistance and high thermal and chemical stability (Raveh *et al*., 2007). To this respect, there are very few candidates do exist, *i.e*. those which form pure or nearly pure covalent bonds. Only the four elements boron, carbon, nitrogen and silicon can form such strong a bonds. (Ehrhardt, 1995). Especially, TiCN had been used as a protective coating material due to its excellent properties such as high melting point, high hardness, and high thermal conductivity (Kim *et al*., 2008; Yashar *et al*., 1999). Ti-based multi-component coatings like TiCN, Ti(BNAl), Ti(SiO) and TiNbCN have been deposited by Physical Vapor Deposition (PVD) magnetron sputtering from composite targets either in an argon atmosphere or reactively in a gaseous argon mixture, nitrogen and methane. Those deposition methods have also been fulfilled by using ion implantation assisted magnetron sputtering (Danen and Sonnenberg, 2003). Take into account that there are a close relationship with the preparation techniques and the deposition parameters on film hardness, in those kinds of materials, hardness enhancement occurs through energetic ion bombardment assisting in crystalline size reduction, grain boundary densification, point defects formation and increase of internal stress. Maximum hardness corresponds to maximum compressive stress and to certain PVD deposition conditions, assuming that the defects responsible for the compressive intrinsic stresses also act as obstacles for dislocation movement thereby increasing the hardness (Raveh *et al*., 2007). Tribological coating evolution has been reviewed by Shtansky *et al*., 2004 where he refers to recent results on the deposition, characterization, testing, and application of multi-component and nanostructured coatings. Optimum performance found in such metal-ceramic films is attributed to the formation of complex quaternary solid solutions (Tretyakov and Mashevskaya, 1999; Qi and Kang, 1998) during deposition processes. In improving the properties of structural materials, Shtanskyet. *et al*., 2004 recommended the use of complex carbonitride solid solutions (master hard coatings) by incorporating both materials such as the nitride and the carbide components in one single phase like CN_x thin films, as re-

ported elsewhere (Riascos *et al.*, 2006). So, in this research the Niobium it was selected in relation to the other elements, *e.g.* Al because the Niobium is a ductile metal, which resists corrosion due to the oxide film. The metal starts to oxidize rapidly in air at 200 oC. Niobium is one of the five major refractory metals (metals with very high resistance to heat and wear). Niobium is used with iron and other elements in stainless steel alloys and also in alloys with a variety of nonferrous metals, such as titanium; moreover, the metal is used in superalloys for jet engines and heat resistant equipment. *(J.C. Caicedo et al, 2010)*

In this way the literature present few researches focused on studying the carbo-nitride quaternary system based on niobium element, therefore, this effect on steel coated with TiCN and TiNbCN has been study and reported by Caicedo *et al*., 2007. In those studies, they found that coated substrates showed a better corrosion resistance. Take in account the above the electrochemical properties with (corrosion resistance) effect on steel uncoated and steel coated with TiCN and TiNbCN the mechanical and tribological properties has not yet been thoroughly studied, due to this synergy problems is highly observed in devices steel with industrial application (*e.g.* machining tools for metal-mechanical factory). The aim of this work is to study the effect of the applied r.f. negative bias voltage on the structure, morphology, mechanical and tribological properties of ternary TiCN with inclusion of Nb element for generating the quaternary TiNbCN coatings deposited by r.f. magnetron sputtering technique on Si (100) and 4140 steel substrates for use in industrial applications.

2. Experimental Details

$TiC_{1-x}N_x$ and $Ti_{1-y}Nb_yC_{1-x}N_x$ films have been grown on silicon (100) and AISI 4140 steel substrates by using a multitarget magnetron reactive sputtering technique, with ar.f. source (13.56 MHz) and two stoichiometric TiC and Nb targets with 99.9% purity. The deposition parameters for obtaining high-quality coatings were sputtering power of 400 W for TiC and 350 W for the Nb target; substrate temperature 300 °C; under circular rotation substrate with 60 RPM, to facilitate the formation of the stoichiometric film.The sputtering gas was a mixture of Ar 76% and N_2 24% with a total working pressure of $6{\cdot}10^3$ mbar, under argon and nitrogen gas flow of 50 sccm and 16 sccm, respectively with a total thickness around 950 nm for all coatings.An unbalanced r.f. bias voltage was applied, which generates a negative signal varying between 0 and -100 V to study their effect upon coating mechanical and tribological properties. The total thickness was measured by a profilometer Veeco Dektak 3030.The crystal structure of the films was determined by using a PANALYTICAL X'Pert PRO X'ray diffractometer with Cu-K_α radiation(α=1.5406 Å).The chemical composition of the films was studied by energy dispersive X-ray (EDX) using a Philips XL 30 FEG(Caicedo *et al*., 2007). Morphology of the surface was observed via Leika 360, Cambridge Instruments Scanning Electron Microscopy (SEM) equipped with an optic light with a magnification range of 525-24.000x and a high sensibility detector (multimode) for scattering electrons. The quantitative elemental concentration depth profile (QDPs) of most of the elements in $TiC_{1y}N_y$ (TiCN) and $Ti_{1x}Nb_xC_{1y}N_y$ (TiNbCN) films were obtained with a LECO glow discharge–optical emission spectrometer (GDOS). The operation conditions were 700 V, 20 mA, and an argon pressure of 7 mbar. The pressure inside the spectrometer was 10^5 mbar, and that in the glow discharge lamp was $3{\cdot}10^2$ mbar. Sputtering with argon ions causes sample erosion with an average rate of 1.84 μm/min in a spotof 4 mm in diameter.TEM microscopy (Philips CM30 and JEOL JEM 1010) operating at 300 kV in all its configurations has been used to investigate and evaluatemicrostructural features of such layers.Hardness and elastic modulus measurements were performed by using a (UBI1-Hysitron) nanoindenter that use a diamond Berkovich indenter tipwith a maximum load of 9 mN. Adherence of the layers was studied by using a Scratch Test Microtest *MTR2* system

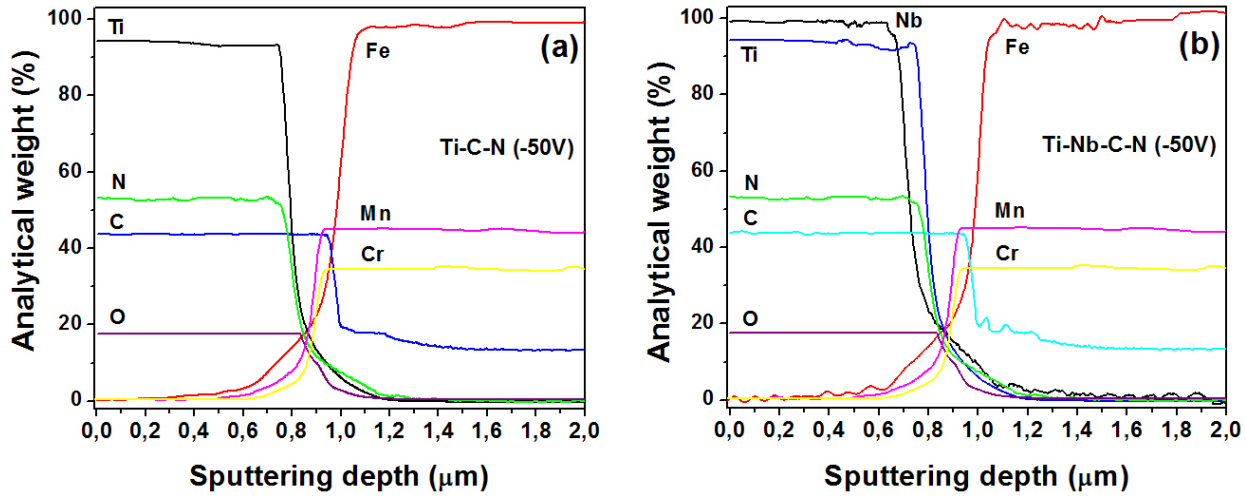

FIGURE 1. Quantitative elemental concentration depth profile: (a) $TiC_{1y}N_y$and (b) $Ti_{1x}Nb_xC_{1y}N_y$ films grown with r.f. negative bias voltages of -50 V.

TABLE I. Stoichiometric relationship and analytical weight percent determined by EDX and GDOS, respectively,for the Ti-C-N and Ti-Nb-C-N films deposited to -50 V.

Technique	Ternary films ($TiC_{1y}N_y$)	Quaternary films ($Ti_{1x}Nb_xC_{1y}N_y$)
EDX	$TiC_{0.16}N_{0.84}$	$Ti_{0.23}Nb_{0.77}C_{0.18}N_{0.82}$
GDOS	$Ti_{(94.12)}$, $C_{(53.20)}$, $N_{(43.63)}$	$Ti_{(93.47)}$,$Nb_{(98.87)}$, $C_{(52.41)}$, $N_{(43.84)}$

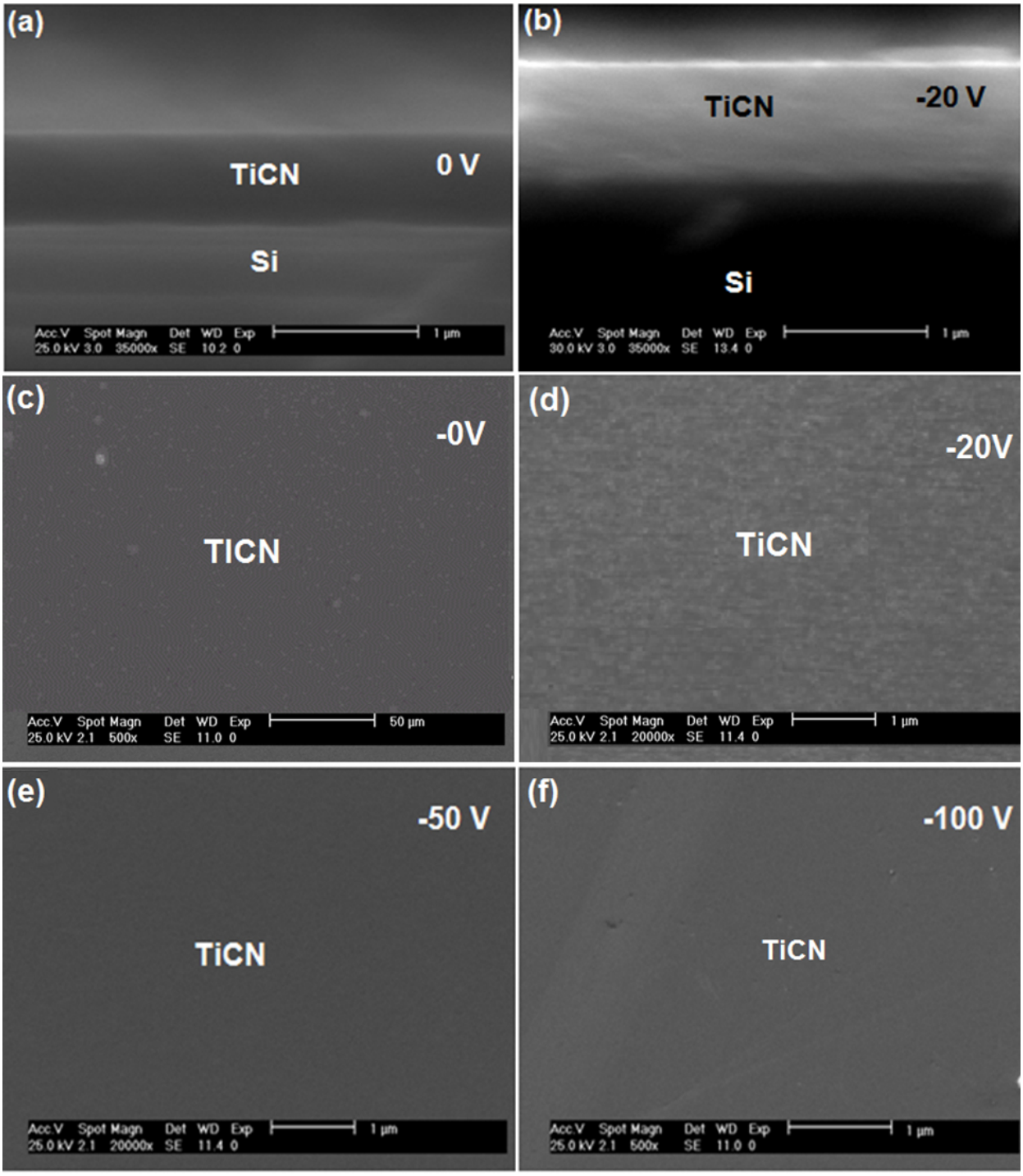

FIGURE 2. Cross sectional and surface SEM micrographs before tribological process for TiCNlayers deposited to 0 and -100 V bias voltage: (a) TiCN (0 V), (b), TiCN (-20 V), (c) surface TiCN (0 V), (d), surface TiCN (-20 V), (e) TiCN (-50 V) and (f) TiCN (-100 V).

the parameters were a scratch length of 6 mm and a raising load of 0-90 N. To identify the different adherence failures Olympus *PME-3* optic microscopy was used.

3. Results and discussion

3.1. Structural an compositional results

The XRD patterns of the $TiC_{1x}N_x$ coatings deposited on Si (100) for r.f. negative bias voltages from 0 to -100 V indicates that the coatings have a cubic structure with two strong peaks corresponding to the TiCN (200) and (111) planes, indicating a light textured growth along these orientations(Caicedo *et al*., 2007). On the other hands the TiNbCN layers shown two strong peaks associate to (200) and (111) planes for both coatings (TiCN and TiNbC N); the reason for these crystalline behaviour is related to a larger number of oriented crystallites in (200) and (111) directions, therefore the oriented crystallites generates more constructive reflections for these crystallographic planes which produce a strong increase in intensity signal.Other physical effect exhibited in the XRD patterns for both Ti-C-N and Ti-Nb-C-N coatings deposited at negative r.f. bias voltages between 0 and -100 V is a slight shift of the peak positions to lower angles (smaller lattice parameter). This is due probably to the increase in the compressive residual stress generated by the bias voltage(Caicedo *et al*., 2007).

Additionally, the effect of the r.f. negative bias voltage on the stoichiometric relationship for all TiCN and TiNbCN layers exhibit a decreasing for carbon content as function of increasing of applied negative bias voltage such as was reported in our previous work (Caicedo *et al*., 2007).

3.1.1. Quantitative elemental concentration depth profile via GDOS analysis

TiC, TiN and NbN GDOS standards were used to obtain the quantitative elemental concentration depth profile. Each single analytical point of the GDOS profile corresponds to the result of the simultaneous integration of each characteristic radiation line emitted during the erosion of a sample layer with a thickness of around of 800 nm for TiCN and 900 nm for TiNbCN films. The profiles in Fig. 1a for TiCN show that titanium, carbon and nitrogen contents remain constant from the film surface toward the film-steel substrate. In the interface film-steel substrate the titanium, carbon and nitrogen contents decrease while the iron, manganese and chromium contents increase, indicating that the film and steel substrate differ markedly in composition (Pancielejko *et al*., 2004). The profiles in Fig. 1b for TiNbCN films show that niobium contents also remain constant from the film surface toward the interface film-steel substrate and in the interface film-steel substrate the niobium contents decrease until steel surface (Balaceanu *et al*., 2009).

It can be observed, in both results for Ti-C-N and Ti-Nb-C-N coatings that little oxygen content was associated to contamination from residual oxygen within PVD reactor, so, when the chemical quantifications are carried out without oxygen contribution, it is possible to find the stoichiometric composition, therefore, the chemical quantifications via quantitative elemental concentration depth profile (QDPs) is in agreement with EDX results (Table I).

3.2. Morphologic analysis via SEM for $TiC_{1x}N_x$ and $Ti_{1y}Nb_yC_{1-x}N_x$ monolayercoatings

The surface and morphology for the layers before any mechanical or tribological test were observed via scanning electron microscopy (SEM). Figure 2 show cross sectional SEM micrographs for Ti-C-N ternary layer with variation in negative bias voltage to 0 V and -20 V (Fig. 2a and Fig. 2b, respectively) which is possible to observe the film-substrate interface, and besides is appreciable the layers continuity a long to the cross sectional without cracks and severe strains. The layer thickness observed by these micrographs is similar to the determined by means of GDOS (850 nm). Figures 2c-2f show a surface SEM image for Ti-C-N layers deposited to 0 V, -20 V, -50 V and -100 V bias voltage, respectively. The uniform dark contrast in the micrographs led to us a clear determination not only of the surface nature from these layers; reflected in a well defined and continue surface free of the pores and cracks but also ina constant stoichiometry in the films, which fix with the EDX results made for all layers.

Figures 3a and 3b show cross sectional SEM micrographs for Ti-Nb-C-N quaternary layer deposited with variation in negative bias voltage to 0V and -20V, respectively. From these images is possible to observe the film-substrate interface, and the layers continuity a long to the cross sectional without cracks and severe strains.The layer thickness observed by these micrographs is similar to the determined by means of GDOS (900 nm). Figures 3c-3f show a surface SEM image for Ti-Nb-C-N layers deposited to 0 V,-20 V, -50 V and -100 V bias voltage, respectively. As the case of the ternary layer, the uniform dark contrast in the micrographs led to us a clear determination not only of the surface nature from these layers; once again reflected in a well defined and continue surface free of the pores and cracks but also in a constant stoichiometry in the films, which fix with the EDX results made for all layers.

3.3. Structural analysis by mean of TEM for $TiC_{1x}N_x$ y $Ti_{1y}Nb_yC_{1-x}N_x$ monolayer coatings

Figure 4 and 5 shows a cross section TEM micrograph of the TiCN and TiNbCN layers deposited onto Si substrate to -50 V. From those image is possible to observe the silicon atomic planes and the film-substrate interface, which is composed for a thin amorphous layer of silicon oxide (Si_xO_y) with a thickness of 2 nm, that oxide layer is formed naturally due to the interaction between the ambient oxygen and the surface from silicon substrate. For both images with high-resolution TEM measurements were performed to further characterize the TiCN and TiNbCN crystalline microstructures. On the other hand, TEMin diffraction mode, *i.e.* converge beam

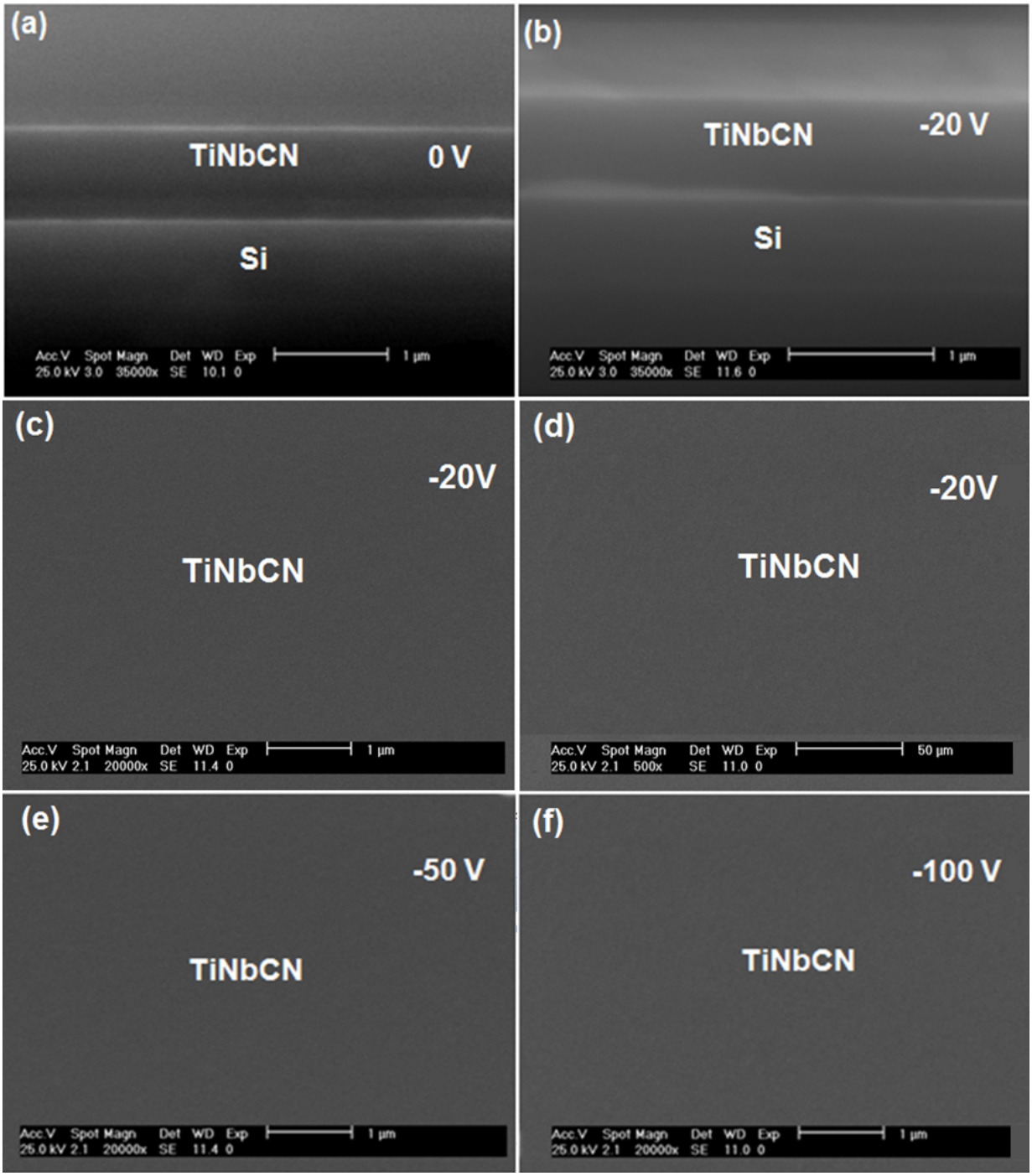

FIGURE 3. Cross sectional and surface SEM micrographs before tribological process for TiNbCN layers deposited to 0 and -100 V bias voltage: entre 0 y -100 V: (a) TiNbCN (0 V), (b), TiNbCN (-20 V), (c) surface TiNbCN (0 V), (d), surface TiNbCN (-20 V), (e) TiNbCN (-50 V) and (f) TiNbCN (-100 V).

electronic diffraction (CBED) was employed with the aim to obtain information about the crystallographic planes, specifically, the interplanar distance (d) corresponding to TiCN and TiNbCN in a preference crystallographic direction. In that sense, it was determined for the TiCN layer an interplanar distance of 2.24497Å in the (100) crystallographic direction, which is consistent with the reported value in JCPDF-03-065-9875 indexation base, while for the TiNbCN layer an interplanar distance of 2.5091Å in the (111) crystallographic direction, which is consistent with the reported value in JCPDF-01-071-6043 indexation base. Other crystallographicorientations like (200) and (220) for the TiCN layer and (200) and (220) for the TiNbCNlayers were possible to identify as was determined by mean of X-ray diffractions results analysis(Caicedo *et al*., 2007).

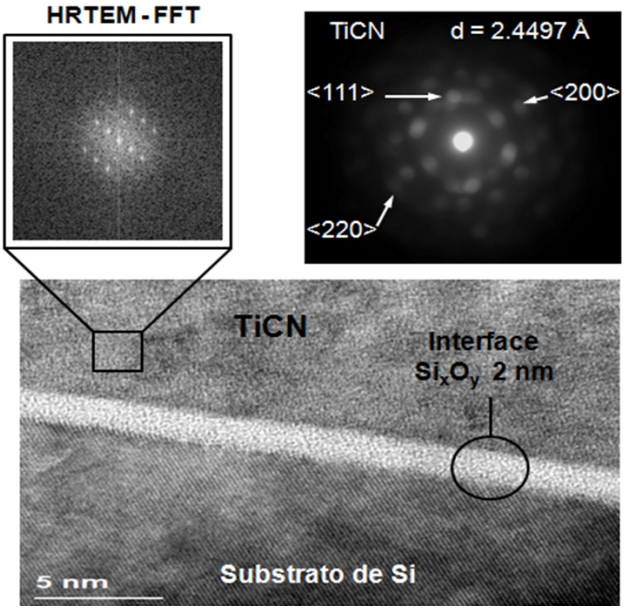

FIGURE 4. Cross section TEM micrograph for the TiCN layer deposited to -50 V, showing the atomics planes when the diffraction of the material is obtained.

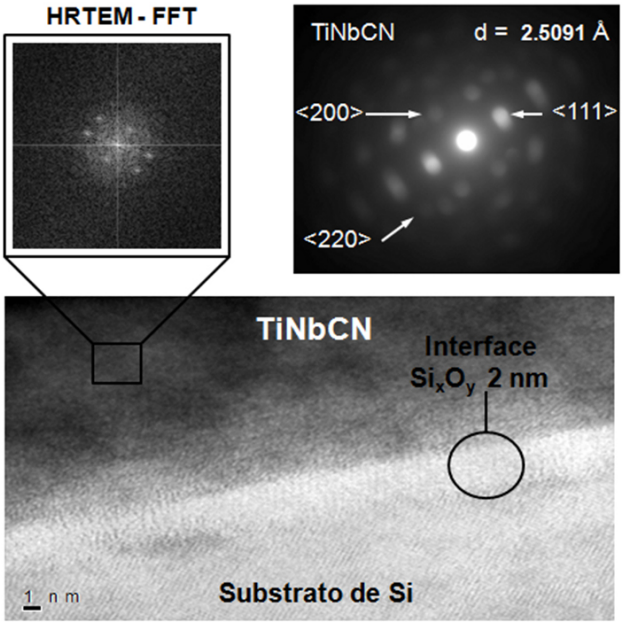

FIGURE 5. Cross section TEM micrograph for the TiNbCN layer deposited to -50 V, showing the atomics planes when the diffraction of the material is obtained.

3.4. Mechanical properties

From nanoindentation measurement was possible to obtain the typical load-displacement indentations curves of the monolayer films using the standard Berkovich indenter. The values of elasticity modulus, E_r, and hardness, H, were obtained by using Oliver and Pharr's method (Oliver and Pharr, 1992). According with Kim *et al*., 2003 there is a relationship between elasticity modulus and hardness called plastic deformation resistance (H^3/E^2 ratio), this relation was calculated for all layers in function of the bias voltageand showed in Fig. 6a. On the other hand from the load-displacement curves is possible to determine the elastic recovery values which is defined by:

$$R = \frac{\delta_{\max} - \delta_p}{\delta_{\max}} \tag{1}$$

where $\delta_{\max}$ is the maximum displacement and δ_p, the residual or plastic displacement (Hajek *et al*., 1997). The equation data were taken from the load-penetration depth curves of indentations for each film and plotted in Fig. 6b.

Figure 6a, show a considerable increment in the resistance to the plastic deformation as function of increment of the bias voltage, this fact is due to the hardness and the elasticity modulus also increase as the bias voltage increase for both coatings. Comparing both coatings for the same bias voltage is observed that the quaternary material show a higher value of the plastic deformation resistance than ternary material. This enhancement in plastic deformation resistance occurs through energetic ion bombardment assisting in crystalline size reduction, grain boundary densification, point defects formation and increase of internal stress which increasing the hardness of the films (Raveh *et al*., 2007).

In Fig. 6 it is observed the mechanical properties in function of the bias voltage where the $Ti_{1y}Nb_yC_{1-x}N_x$ coatings present a curve shift toward high values for the plastic deformation resistance (which includes hardness and elastic modulus) as compared with the $TiC_{1x}N_x$ coatings. This effect occurs because the niobium exerts a substitutional displacement on some titanium ions to form a stable NaCl-type FCC structure; thus, providing a variation in the Burger's vector of the $Ti_{1y}Nb_yC_{1-x}N_x$ material and showing a different elasto-plastic properties, because titanium has an ionic radius of 0.68 (Å) different to niobium ionic radius of 0,70 (Å). The Nb inclusion improves the mechanical properties exhibiting higher hardness when ions polarize the surface of $Ti_{1y}Nb_yC_{1-x}N_x$ coatings as compared with $TiC_{1x}N_x$ coatings.

Moreover Fig. 6b illustrates the behavior of the elastic recovery (R) as the bias voltage change from 0 to -100 V. From this figure it was determine an increase at 24% in elastic recovery for the TiNbCN layer respect to the TiCN layer at the maximum bias voltage applied (-100V). This effect is clearly correlated to the increased film density, hardness and surface smoothness due to the inclusion of the Nb atom into the TiCN structure, which change the internal stress to higher values as the negative bias voltage is varied (Caicedo *et al*., 2007).

3.5. Adherence analysis by using a critical load criterion

The scratch test technique was carried out to characterize films adherence strength. The adhesion properties of monolayer coatings can be characterized by the following two terms, L_{C1}, the lower critical load, which is defined as the load where first cracks occurred (cohesive failure) and the

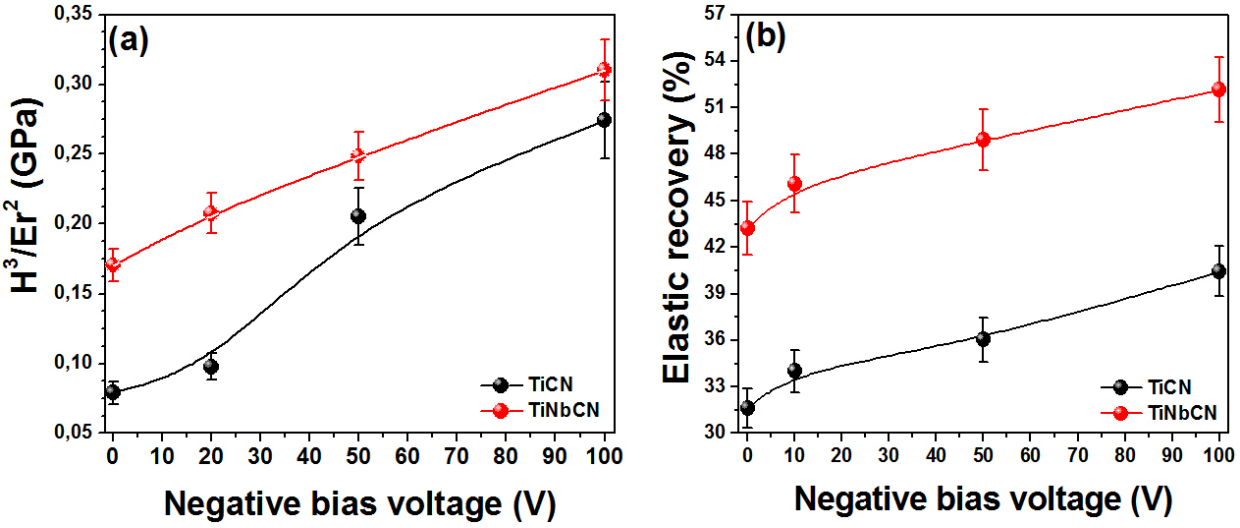

FIGURE 6. Elasto-plastic properties for $TiC_{1x}N_x$ and $Ti_{1y}Nb_yC_{1-x}N_x$ layers deposited with bias voltage between 0 and -100 V; (a) plastic deformation resistance and (b) elastic recovery (R).

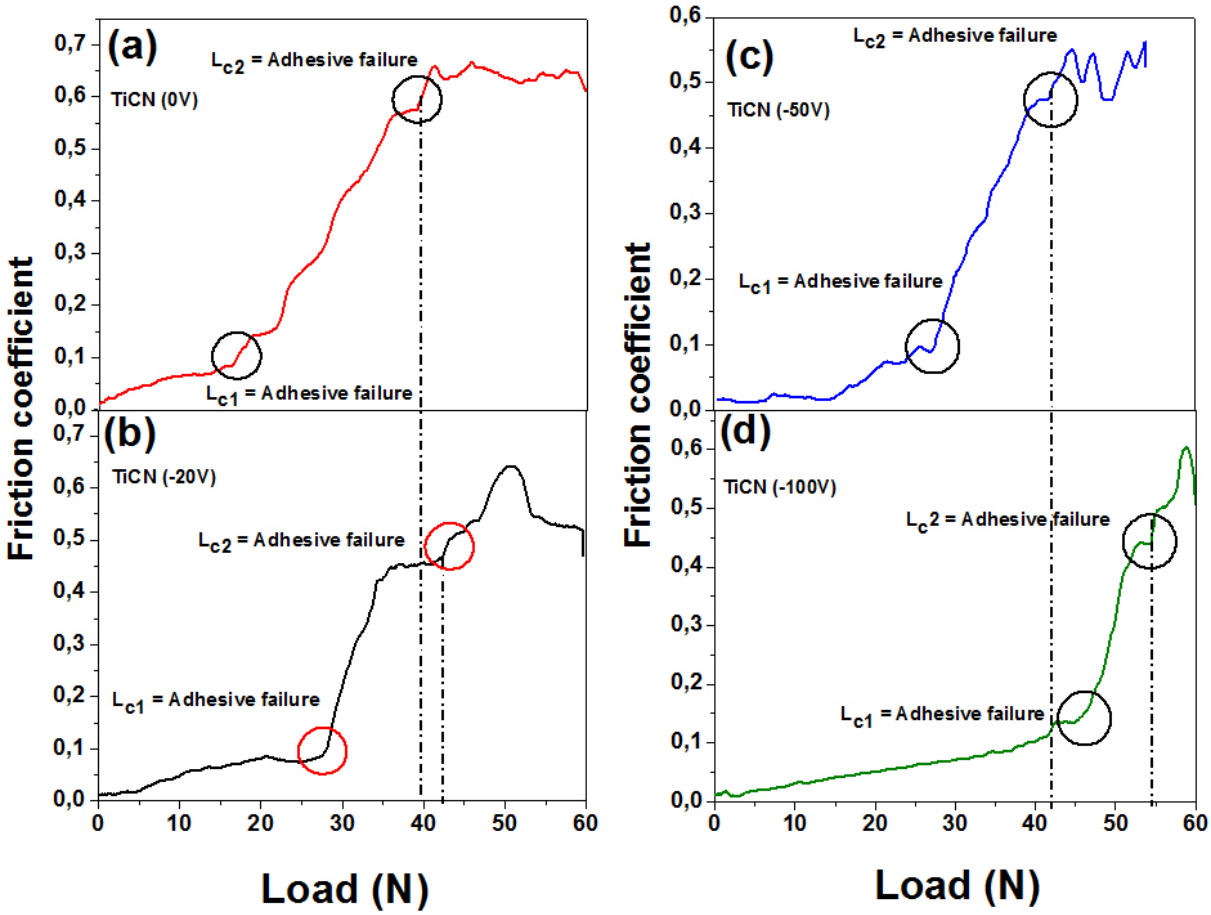

FIGURE 7. Tribological results for friction coefficient curves versus applied load, showing the adhesion failure (L_{C2}) for the TiCN monolayer: (a) 0 V, (b) -20 V, (c) -50 V and (d) -100 V.

L_{C2}, the upper critical load, which is the load where the first delaminating at the edge of the scratch track occurred (adhesion failure) (Hedenqvis *et al*., 1997).

In this work those critical loads were determined experimentally plotting friction coefficient versus applied load. From this graphics L_{C1} and L_{C2} correspond to zones where

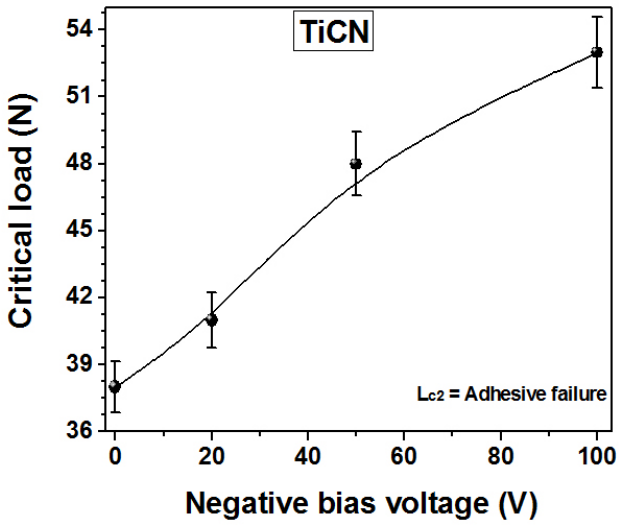

FIGURE 8. Critical load (adhesive failure) correlation with the applied bias voltage for the TiCN layer.

the friction is independent of the applied load. For discussing the behavior of the critical load in the adhesive failure for the layers in dependence to the bias voltage, it was took the approach formulated by Bull *et al.*, 1997 referring to thedifferent variables that are implying in a scratch test as follow:

$$Lc = \frac{A}{\nu \cdot \mu}\sqrt{\frac{2 \cdot Er \cdot Wa}{t}} \qquad (2)$$

where $_{LC}$is the critical load, ν is the Poissons' ratio of the coating material, A is the cross-sectional area of the scratch, μ is the coefficient of friction which coating detachment occurred, $W_a$is the reversible work of adhesion, t is the thickness of the film and$E$ris the Youn's modulus of the film.The values of critical load (L_{C1} and L_{C2}) for the TiCN layers deposited to different bias voltage are shown in Fig. 7. The L_{C1} values for the monolayer coatings were in the range of 16-45 N; the highest value was attributed to the TiCN layer deposited to -100 V.

The adhesive failure (L_{C2}) is the most important factor because from this value the coating loose completely functionality and the properties *e.g.* tribological response depend of the substrate. The L_{C2} values for the TiCN layers deposited with different bias voltageare summarized in Fig. 8. In this study, it was observed an increase at 28% in the L_{C2} for the TiCN layer deposited to -100 V respect to the same layer deposited to 0 V.

For the TiNbCN layers deposited with bias voltage between 0V and -100 V, the values of critical load (L_{C1} and L_{C2}) are shown in Fig. 9. For this material the L_{C1} values

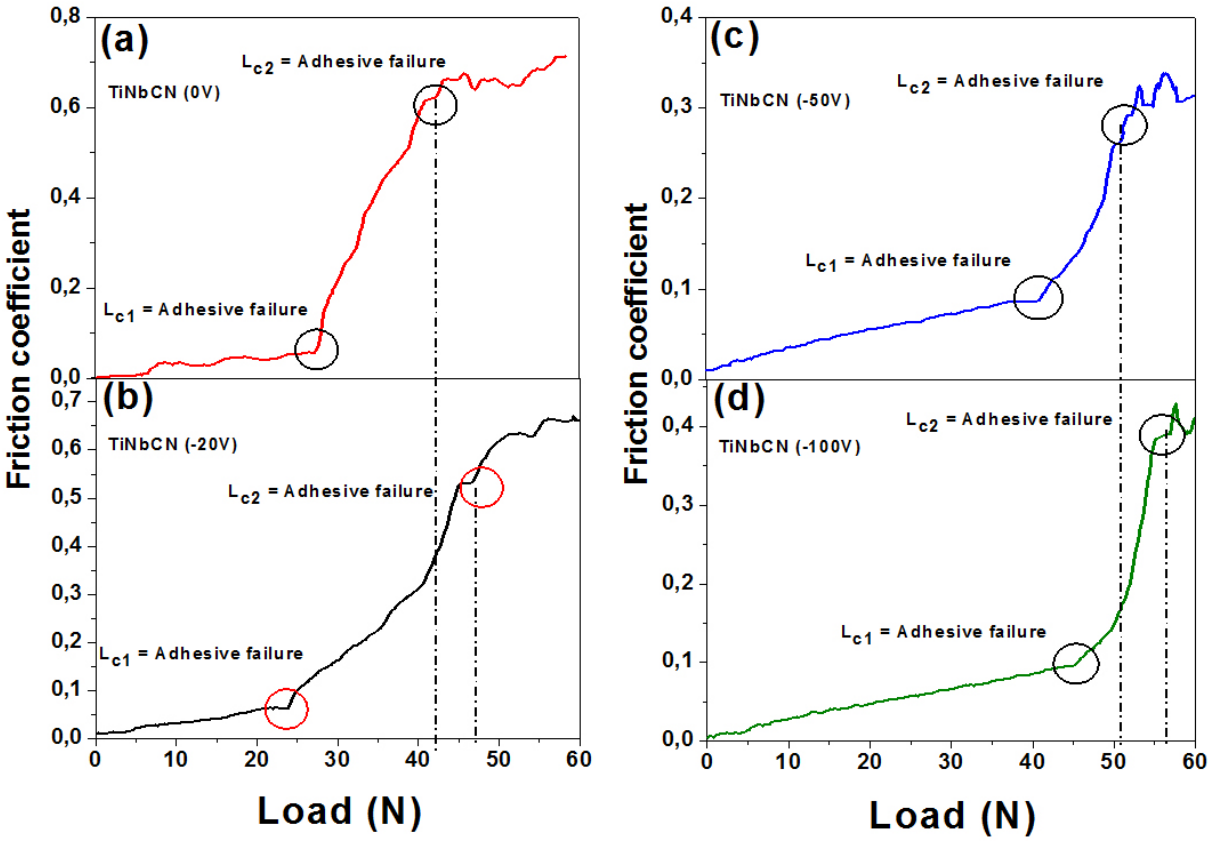

FIGURE 9. Tribological results for friction coefficient curves versus load applied, showing the adhesion failure (L_{C2}) for the TiNbCN layer: (a) 0 V, (b) -20 V, (c) -50 V and (d) -100 V.

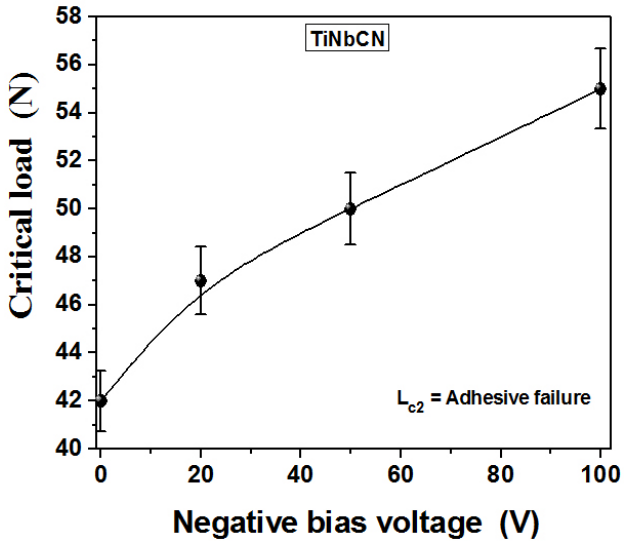

FIGURE 10. Critical load (adhesive failure) correlation with the applied bias voltage for the TiNbCN layer.

were in the range of 28-46 N; once again the highest value was attributed to the layer deposited to -100 V.

The L_{C2} values for the TiNbCN layers deposited with different bias voltageare shown in Fig. 10. For this material, it was observed an increase at 26% in the L_{C2} for the TiNbCN layer deposited to -100 V respect to the same layer deposited to 0 V.

From Fig. 8 and 10 values is possible to observe that the TiNbCN layer deposited to -100 V represent an increase of the 3% of the critical load in relation with the TiCN layer deposited with the same bias voltage, that fact could be associated with the introduction of the Nb atom into TiCN structure, which modify the field of stress in the growing layer due to the modification in the lattice parameter, changing on this way the mechanical and tribological response.

The behavior reported for the critical load in this study could be explained through the Eq. (2). For a material with ν valueconstant,t would be obvious that at the same applied loading rate and an identical moving speed of the scratch indenter as well as to the same layer thickness, t, and a short range of the friction coefficient for the tribological pair, μ the coatings deposited at various conditions exhibited quite different responses. For our TiCN and TiNbCN layers the scratch area, A, decrease as the voltage bias was increased, indicating that the critical load was governed by the elastic-plastic response from the film and the adhesion in the film-substrate interface.Therefore from plastic deformation resistanceand elastic recovery values is possible to say that the enhancement in critical load for the layers occurred due to the effect of the energetic ion bombardment which not only improve the adhesion assisting in crystalline size reduction and grain boundary densification, but also enhancement the mechanical response by point defects formation and increase of internal stress(Burnett and Rickerby, 1987). Therefore assuming that the defects responsible for the compressive intrinsic stresses also act as obstacles for dislocation movement it will be necessary a higher load to make cracks and pull up the layer (adhesive failure) as was showed is this study for both materials.

3.5.1. Surface tribological analysis

Optical microscope images showing the different behaviors of the TiCN and TiNbCN monolayer coatings after scratching are showed in Fig. 11a-b. The figures revealed that different types of adhesive layer/substrate failures appear under strong plastic deformation conditions. It was possible to identify some of the failure mechanism that affects the coating-substrate system.On the pictures frame scratch Fig. 11a and Fig. 11b for the TiCN and TiNbCN layers, respectively, it

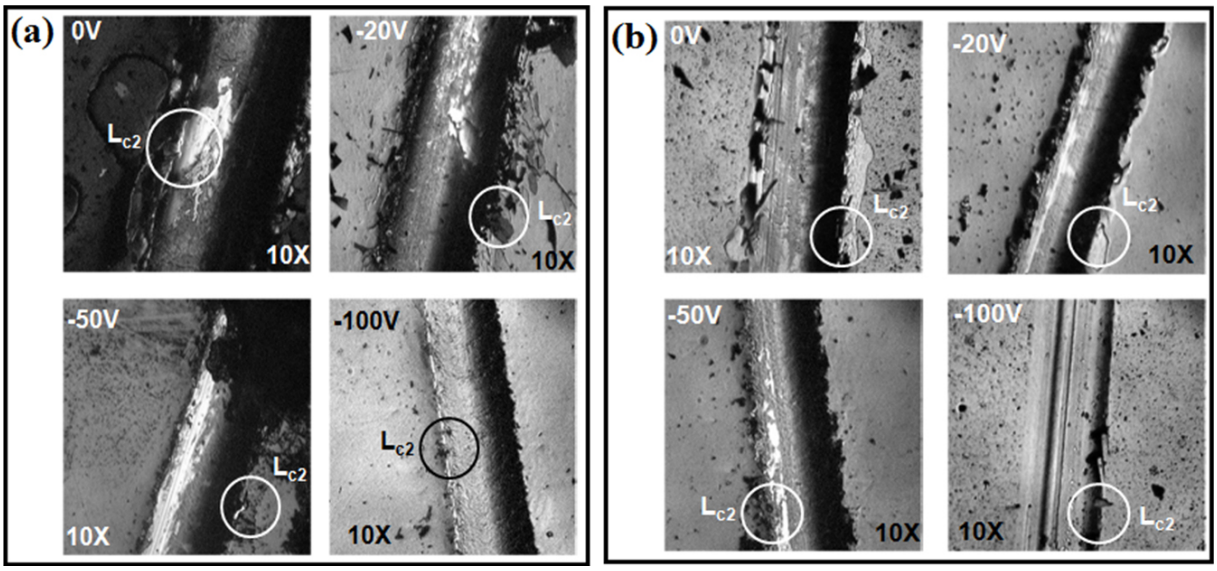

FIGURE 11. Optical microscope images at 10X of scratch tracks on (a) TiCN and (b) TiNbCN monolayer coatings deposited onto AISI 4140 steel substrates with different bias voltage.

can be observed two failure types, the first one is associated to internal transverse cracking at the beginning of the scratch and sideward lateral flanking in the final part of the scratch denominate as adhesive failure (L_{C2}), the second one failure type is occurred due to the accumulation of stress at the scratch edges(Holmberg *et al*., 1994). This last behavior was more notorious for lower critical load associated to both layers deposited to 0 V, which shown a premature failure.

4. Conclusions

$TiC_{1-y}N_y$ and $Ti_{1-y}Nb_yC_xN_{1-x}$coatings were deposited by reactive r.f. magnetron sputtering by using simultaneous deposition from TiC and Nb targets in N_2+Ar mixture. The r.f. negative bias voltage in the coatings was varied by changing the applied potential on the substrate from 0V to -100V generating a slightly shift of the peak positions to lower angles, due to the increase in the tensile residual stress at higher voltages. The r.f. bias application induces important formation of crystallographic phases such as FCC (111) and (200) (Caicedo *et al*., 2007).

The lowest critical load in the coatings was found for the r.f. negative bias applied of -100 V, observing enhancements of the tribological properties by reduction of the friction coefficient in 28 % for Ti-C-N and 26 % for Ti-Nb-C-N coatings when both coatings were compared with the same deposited to 0 V, therefore, a high critical load for adhesive failure was obtained in coatings due to two factors: growth with highest applies negative bias voltage which produce the increasing of the density, (and therefore of the hardness), and the niobium inclusion into the FCC structure, changed the crystal structure, improving the mechanical properties.

Finally, high hardness combined with carbon content lubricant presence confers to TiCN and TiNbCN coatings a successful sliding wear behavior compared to TiNC and TiNbCN coatings growth in absence of applied r.f. negative bias voltage (0 V).

Acknowledgements

This research was supported by "El patrimonio Autónomo Fondo Nacional de Financiamiento para la Ciencia, la Tecnología y la Innovación Francisco José de Caldas" under contract RC-No. 275-2011 with Center of Excellence for Novel Materials (CENM). Moreover, the authors acknowledge the Serveis Científico-Técnics of Universitat de Barcelona. For the TEM results.

1. J.C. Caicedo *et al*., *Appl. Surf. Sci.* **256** (2010) 2876.
2. AviRaveh, Ido Zukerman, RoniShneck, Rudi Avni, and Ilana Fried, *Surf. Coat. Technol.* **201** (2007) 6136.
3. H. Ehrhardt, *Surf. Coat. Technol.* **74-75** (1995) 29.
4. B.S. Kim, G.S. Kim, S.Y. Lee, and B.Y. Lee, *Surf. Coat. Technol*. **202** (2008) 5526.
5. G. Zambrano *et al*., *Surf. Coat. Technol.* **108-109** (1998) 323.
6. P.C. Yashar and W.D. Sproul, *Vacuum* **55** (1999) 179.
7. E.H.J. Danen and A Sonnenberg, *J. Pathol* **201** (2003) 632.
8. D.V. Shtansky, *Nanostructured Thin Films and Nanodispersion Strengthened Coatings*, 1st ed. (Springer, Moscow, Russia, 2004). pp. 155-166.
9. V.I. Tretyakov, and V.L. Mashevskaya, *Powder Metall. Met. Ceram*. **38** (1999) 64.
10. F. Qi, and S. Kang, *Mater. Sci. Eng. A.* **251** (1998) 276.
11. H. Riascos, J. Neidhardt, G.Z. Radnoczi, J. Emmerlich, G. Zambrano, L. Hultman, and P. Prieto, *Thin Solid Films* **497** (2006) 1.
12. M. Pancielejko, and W. Precht, *J. Mater. Process. Technol.* **157** (2004) 394.
13. M. Balaceanu *et al*., *Solid State Sciences* **11**, (2009) 1773.
14. W.C. Oliver, and G.M. Pharr, *J. Mater. Res.* **7** (1992) 1564.
15. G.S. Kim, S.Y. Lee, and J.H. Hahn, *Surf. Coat. Technol.* **171** (2003) 91.
16. V. Hajek, K. Rusnak, J. Vlcek, L. Martinu, and H.M Hawthorne, *Wear* **213** (1997) 80.
17. P. Hedenqvis and S. Hogmark, *Tribology International* **30** (1997) 507.
18. S.J. Bull, D.S. Rickerby, A. Matthews, A. Leyland, A.R Pace, and J. Valli, *Surf. Coat. Technol.* **36** (1988) 503.
19. P.J. Burnett, and D.S. Rickerby, *Thin Solid Films* **15** (1987) 403.
20. K. Holmberg, and A. Matthews, *COATINGS TRIBOLOGY Properties, Techniques and Applications in Surface Engineering*, 1st ed. (ELSEVIER, Gt. Britain, 1994). pp. 40-50.